Journal of Statistical Physics, Vol. 107, Nos. 1/2, April 2002 (© 2002)

A Lattice Boltzmann Model for Anisotropic Crystal Growth from Melt

W. Miller[1] **and S. Succi**[2]

Received February 12, 2001; accepted August 5, 2001

We coupled the lattice Boltzmann method with enhanced collisions for hydrodynamics with a model for the anisotropic liquid/solid phase transition. The model is based on a simple reaction model. As a test we have performed calculations for dendritic growth of a crystal into an undercooled melt.

KEY WORDS: Lattice Boltzmann equation; dendrites; crystal growth.

1. INTRODUCTION

Crystal growth from melt plays an important role in industrial processes as well as in nature. The growth of large single crystals of high quality for opto-electronic purposes is an industrial process of major importance. Often, the macroscopic growth is strongly influenced by microscopic processes. For instance, the growth of twinned crystals, which do not have the proper opto-electronic properties as a single crystal, might be caused by defects on atomistic scale. It is therefore of great interest to couple effects on the microscopic scale with those on the macroscopic.

When a small seed crystal is placed or nucleates in an undercooled melt, the solid phase grows rapidly. Directional anisotropies of surface and kinetic energies, due, e.g., to the underlying molecular geometry, result in preferred growth directions and the development of dendrites.(1) Experiments show that the growth velocities and the structure depend strongly on the angle between crystal and gravity direction.(2) Nevertheless, theoretical

[1] Institut für Kristallzüchtung (IKZ), Max-Born-Str.2, 12489 Berlin, Germany (An institute of the Gottfried Wilhelm Leibniz Society, WGL); e-mail: wm@ikz-berlin.de

[2] Istituto per le Applicazioni del Calcolo (C.N.R.), Viale del Policlinico 137, Rome 00161, Italy.

0022-4715/02/0400-0173/0 © 2002 Plenum Publishing Corporation

and numerical studies focused for a long time only on cases without convection. Only recently forced flow in refs. 3 and 4 or thermal flow in ref. 5 has been included in the calculations based on differential equations in a continuum framework. The sharp interface limit for the phase-field model with convection has been very recently invented by Anderson *et al.*[6] In this paper we present a different approach to the problem: we use the lattice Boltzmann method for the hydrodynamics extended by a model for the phase transition, which is based on an analogy to chemical reactions. The aim is to calculate both the phase transition and the hydrodynamics on a mesoscopic scale.

2. HYDRODYNAMICS

In the late 1980's the first lattice fluid models for hydrodynamics were introduced.[7] They mimic the hydrodynamics by means of fictitious quasi-particles hopping from one lattice site r_* to the next and undergoing collisions at each site. Here we concentrate on the description of the lattice Boltzmann method with enhanced collisions on a face-centred hypercubic (FCHC) lattice as introduced by Higuera *et al.*[8] In the four-dimensional FCHC lattice the motion of the lattice fluid particles is restricted to 24 directions, which define the links between a node and its adjacent ones (Fig. 1). Therefore, the lattice fluid consists of 24 quasi-particles, defined at a node $\vec{r}_*$ with a distribution function $N_i(\vec{r}_*, t_*)$. The index i labels the direction, the speed of a particle is $\vec{c}_i$ with $|\vec{c}_i| = \sqrt{2}\,\Delta t$, where Δt is the discrete timestep. We set the timestep to unity ($\Delta t = 1$) so that each moving

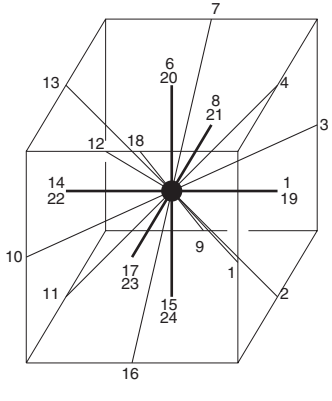

Fig. 1. Unit cell of the lattice Boltzmann model on the face-centred hypercubic (FCHC) lattice. The links in x, y, and z direction drawn in thick lines split into two links for positive and negative direction of the fourth dimension, respectively.

quasi-particle is hopping to the next node in a timestep. In addition to the moving quasi-particles we have particles of zero speed (rest particles) to ensure the Gallilean invariance.[9] We denote the density of rest particles with d_0 and that of the moving particles with d, so that the total (average) density of the lattice fluid per node is $\rho^* = d_0 + 24d$. The local density is given by

$$\rho^*(\vec{r}_*, t_*) = \sum_i N_i(\vec{r}_*, t_*) \tag{1}$$

and the velocity of the lattice fluid by

$$\vec{u}^*(\vec{r}_*, t_*) = \frac{1}{\rho^*} \sum_i \vec{c}_i N_i(\vec{r}_*, t_*) \tag{2}$$

The particle distributions evolve via a discretized and simplified Boltzmann equation:

$$N_i(\vec{r}_* + \vec{c}_i, t_* + 1) = N_i(\vec{r}_*, t_*) + \sum_j \mathscr{A}_{ij}[N_j(\vec{r}_*, t_*) - N_j^{eq}(\vec{r}_*, t_*)] + F_i \tag{3}$$

All entities like density, velocity, forces are measured in lattice units (l.u.). A physical problem is defined by a set of dimensionless numbers like, e.g., Reynolds number or Grashof number, which read in terms of the lattice Boltzmann model $Re = u_0^* N / \nu_*$ and $Gr = \beta \, \Delta T^* N^3 / \nu_*^2$, respectively. Here, N is the number of nodes for the characteristic length, u_0^* and ΔT^* are the characteristic velocity and the characteristic temperature difference in lattice units, respectively, β is a parameter, which enters the buoyancy force $\vec{F}^B = \beta T^* \vec{n}_g$, where $\vec{n}_g$ is a unit vector in the direction of the gravity. This force enters Eq. (3). N_i^{eq} is the local equilibrium distribution, $\mathscr{A}_{ij}$ the collision matrix, and F_i is the component of an additional force $\vec{F}^*$ to be detailed later. The equilibrium distribution is

$$N_i^{eq} = d + \frac{\rho^*}{24}[2(c_i)_\alpha \, u_\alpha^* + 3(c_i)_\alpha \, (c_i)_\beta \, u_\alpha^* u_\beta^* - (u^*)^2] \tag{4}$$

for the moving particles and

$$N_i^{eq} = d_0 - \frac{\rho^* u^{*2}}{2} \tag{5}$$

for the rest particles,[10] which ensures that we obtain the Navier–Stokes equations in the continuum limit. The collision matrix is symmetric and has

a leading eigenvalue $\lambda = -1/\tau$,[11] where τ is the relaxation time of the lattice fluid, which is related to the viscosity ν_*:

$$\tau = 3\nu_* + \tfrac{1}{2} \tag{6}$$

The FCHC lattice has in total four dimensions so that three can be used to obtain the real velocity components (u_x^*, u_y^*, u_z^*) and the fourth dimension can be used to solve the transport equation for a scalar.[7, 12] If we do not allow any variation in the fourth direction, the Navier–Stokes equation for the velocity component u_4^* reads:

$$\frac{\partial u_4^*}{\partial t} + (\vec{u}^* \cdot \nabla)\, u_4^* - \nu \nabla^2 u_4^* = 0 \tag{7}$$

This is the transport equation for a scalar u_4 with unit Prandtl/Schmidt number. A non-unit Prandtl/Schmidt number can be achieved with a modification of the collision matrix by introducing a second relaxation time $\tau_2 = 3D^* + \frac{1}{2}$, where D^* is the diffusivity of the scalar in l.u.[13, 14] In this paper we treat the temperature T^* as a scalar, i.e., we indentify u_4^* with T^*. Other authors use a thermal LBM,[15, 16] where the total energy is computed, but besides a larger computational cost these schemes are numerically stable only in a very limited parameter space.

3. PHASE TRANSITION

In the framework of continuum models phase-field methods have become very popular. They are based on the Landau–Ginzberg theory and were introduced by Caginalp in 1985.[17] Later they were extended to anisotropic growth.[18, 19] Recently they are used intensively for the calculation of the dendrite growth.[3, 4, 20, 21] The solid and liquid phase is distinguished by a phase field ϕ (solid: $\phi = -1$, liquid: $\phi = +1$), whose time evolution is given by a Landau–Ginzburg-like differential equation. This equation is derived from a free energy with a double-well potential and a second order bending term. Because the height of the double-well potential is normally hard to define by physical data, the width δ of the transition region is fixed and a parameter of the computation.[22] The profile of the phase-field is given by $\phi = \tanh(d/2\delta)$ (d: coordinate normal to the interface, 6δ: thickness of the interface, where $-0.1 \leqslant \phi \leqslant 0.1$), the equation for the phase-field reads:

$$\frac{\partial \phi_s}{\partial t} = \mu_k \Gamma \left[\nabla^2 \phi_s - \frac{\phi_s(1-\phi_s)(1-2\phi_s)}{\delta^2} \right] + \mu_k (T_c - T)\, \frac{\phi_s(1-\phi_s)}{\delta} \tag{8}$$

For convenience we have introduced the solid fraction ϕ_s:

$$\phi_s = 1/2(1-\phi) \tag{9}$$

Γ is the Gibbs–Thomson coefficient and μ_k a kinetic coefficient.

In the discrete lattice model we also use the phase-field as an order parameter but define its evolution by a simple rate equation:

$$\phi(r_*, t_*) = \phi(r_*, t_* - 1) + \mathcal{R}(r_*, t_*) \tag{10}$$

This equation is designed to describe the dynamics of the phase transition on a mesoscopic time scale. In most real cases, the time scale for crystalization/melting is much faster than the time scale for thermal diffusion or hydrodynamics, which were introduced in the previous section via the relaxation times τ and τ_2. Since melting/solidification is an activated process, we postulate the following chemical expression for the reaction term $\mathcal{R}(r_*, t_*)$:

$$\begin{aligned}\mathcal{R}(r_*, t_*) = {} & f_{s\to l} K^{s\to l}(r_*, t_*)\,[1-\phi(r_*, t_*-1)] \\ & - f_{l\to s} K^{l\to s}(r_*, t_*)\,[1+\phi(r_*, t_*-1)]\end{aligned} \tag{11}$$

where $f_{s\to l}$, $f_{l\to s}$ are frequency factors, basically the inverse time scale for solidification/melting respectively, and $K^{s\to l}$, $K^{l\to s}$ are switch functions controlling the onset of solidification/melting around the critical temperature T_c. Their specific form is ($T'(r_*, t_*) = T^*(r_*, t_*) - T_c$):

$$K^{s\to l}(r_*, t_*) = \tfrac{1}{2}\,(1+\tanh\{(T'(r_*, t_*) - T_s)/T_w\}) \tag{12}$$

$$K^{l\to s}(r_*, t_*) = \tfrac{1}{2}\,(1-\tanh\{(T'(r_*, t_*) + T_s)/T_w\}) \tag{13}$$

where T_w controls the energy range of the transition and T_s defines two distinct activation energies for melting and solidification. The tanh is a smooth function to connect the situation of an infinite high to an infinite small barrier for the transition. This corresponds to the picture in a continuum phase-field model, where the double-well potential is distorted by the temperature gradient in the system and the barrier for the transition in one direction is increasing while the one in the other direction is decreasing.

In order to allow the phase transition only at the interface, we modify the switch functions in such a way as to inhibit solidification in the solid phase and melting in the liquid phase:

$$K^{s\to l}(r_*, t_*) \to K^{s\to l}(r_*, t_*)\,\tfrac{1}{8}\sum_i \{\tfrac{1}{2}\,g_i(1+\phi(\vec{r}_* + \vec{c}_i'))\}^2 \tag{14}$$

$$K^{l\to s}(r_*, t_*) \to K^{l\to s}(r_*, t_*)\,\tfrac{1}{8}\sum_i \{\tfrac{1}{2}\,g_i(1-\phi(\vec{r}_* + \vec{c}_i'))\}^2 \tag{15}$$

where $\vec{c}_i'$ is the projection of $\vec{c}_i$ on the physical space, i.e., in two dimensions we have two horizontal and vertical directions with $|\vec{c}_i'| = 1$ and four diagonal directions with $|\vec{c}_i'| = \sqrt{2}$. In order to normalize the contributions to the sum, we introduced the scaling g_i, which takes the value 1 for horizontal and vertical directions and $1/\sqrt{2}$ for diagonal directions. Because the sum runs over all neighbors the rate $\mathscr{R}$ depends now on the phase-field at the surrounding nodes. The square of the curly brackets suppresses a steadily increasing width of the transition region for a moving solidification plane. This corresponds to the approach of a fixed width of the transition region in the continuum phase-field model.[3, 20] As we will see in a moment, using the Eqs. (14) and (15) recovers the continuum phase-field equation in the continuum limit.

The corresponding macrodynamical equation is derived in the same manner as for the original lattice Boltzmann model.[7] We assume that ϕ is changing on a spatial scale ε^{-1} and we introduce the time and space scale $t_1 = \varepsilon t_*$ and $r_1 = \varepsilon r_*$, respectively. Furthermore, we denote the time and space derivative with ∂_t and ∂_r, respectively. Since we have only one time and length scale for the phase transition we can make the substitution $\partial_t \to \varepsilon \partial_{t_1}$ and $\partial_r \to \varepsilon \partial_{r_1}$. We assume $f_{s \to l} \equiv f_{l \to s} = f$ and $T_s = 0$ and use the fact that in the vicinity of the phase transition ($T'/T_w < 1$) tanh is a linear function in its argument. The equation for the phase-field in the continuum space reads:

$$\phi(r, t+\varepsilon) = \phi(r, t) + fK^{s \to l}(r, t)[1-\phi(r, t)] - fK^{l \to s}(r, t)[1+\phi(r, t)] \tag{16}$$

For convenience, we introduce the solid fraction $\phi_s = (1-\phi)/2$. We then get the equation:

$$\phi_s(r, t+\varepsilon) - \phi_s(r, t) = \frac{f}{2} \sum_i g_i \left\{ (1-T'/T_w)(1-\phi_s) \frac{1}{8} \phi_s^2(r+\varepsilon \vec{c}_i', t) - (1+T'/T_w)\, \phi_s \frac{1}{8} [1-\phi_s(r+\varepsilon \vec{c}_i', t)]^2 \right\} \tag{17}$$

We expand ϕ_s in time and space as $\phi_s(r, t+\varepsilon) = \phi_s(r, t) + \varepsilon \partial_{t_1} \phi_s + \mathcal{O}(\varepsilon^2)$ and $\phi_s(r+\varepsilon \vec{c}_i', t) = \phi_s(r, t) + \varepsilon \vec{c}_i' \partial_{r_1} \phi_s + \mathcal{O}(\varepsilon^2)$. Up to first order in ε we get:

$$\partial_t \phi_s = \frac{f}{2} \left\{ (1-T'/T_w)(1-\phi_s) \left[\phi_s^2 + 2\phi_s \varepsilon \frac{1}{8} \sum_i g_i c_{i\alpha}' \partial_{r_1, \alpha} \phi_s \right] - (1+T'/T_w)\, \phi_s \left[1 - 2\phi_s + \phi_s^2 + 2(1-\phi_s)\, \varepsilon \frac{1}{8} \sum_i g_i c_{i\alpha}' \partial_{r_1, \alpha} \phi_s \right] \right\} \tag{18}$$

Because $\sum_i g_i c_i \alpha' \partial_{r_1,\alpha}\phi_s$ is zero, we obtain Eq. (8) without the term of the bending energy of the phase-field:

$$\partial_t \phi_s = \frac{f}{2}\phi_s(1-\phi_s)(2\phi_s-1) - \frac{f}{2}\phi_s(1-\phi_s)\frac{T'}{T_w} \tag{19}$$

We can find the relations $T_w = \Gamma/\delta$ and $f = 2\mu_k T_w/\delta$, where Γ is the Gibbs–Thomson coefficient, μ_k a kinetic coefficient and δ the width of the transition region of the phase field. If $T_s \neq 0$ we get an additional term $T_s/T_w f\phi_s(1-\phi_s)(1-2\phi_s)$. In this case we also should expand the tanh like $\tanh(x) \approx x/(1+x^2/2)$. Assuming $T' \ll T_s$ we expand

$$\tanh\{(T'(r_*, t_*) \pm T_s)/T_w\} \approx \frac{T'(r_*, t_*) - T_s}{T_w\left(1+\frac{1}{2}\frac{T_s^2}{T_w^2}\right)}$$

Performing the continuum limit with this expression we obtain the following relation for the Gibbs–Thomson coefficient:

$$\Gamma = \delta\left[T_w\left(1+\frac{1}{2}\frac{T_s^2}{T_w^2}\right) - T_s\right] \tag{20}$$

This relation holds only if Γ is measured at a point where T' is small compared to T_w and T_s.

We now consider the second order terms. Again we assume $T_s = 0$ and expand the tanh linearly in its argument. Then the expansion yields:

$$\begin{aligned} 2\varepsilon^2\partial_{t_2}\phi_s = \tfrac{1}{8}\varepsilon^2 \sum_i \{&(1-2\phi_s)(d_{i\alpha}\partial_{r_1,\alpha}\phi_s)^2 + \phi_s(1-\phi_s)\, d_{i\alpha}d_{i\beta}\partial_{r_1,\alpha}\partial_{r_1,\beta}\phi_s \\ &+ T'/T_w(-(d_{i\alpha}\partial_{r_1,\alpha}\phi_s)^2 + \phi_s(\phi_s-1)\, d_{i\alpha}d_{i\beta}\partial_{1r,\alpha}\partial_{r_1,\beta}\phi_s)\} \end{aligned} \tag{21}$$

Here we introduced a second time scale t_2 and the multi-scale formalism for the time derivative reads now: $\partial_t \to \varepsilon\partial_{t_1} + \varepsilon^2\partial_{t_2}$. With the relations $\sum_i g_i d_{i\alpha}d_{i\beta}\partial_{r_1,\alpha}\partial_{r_1,\beta} = 4\nabla^2\phi_s$ and $\sum_i g_i(d_{i\alpha}\partial_{r_1,\alpha}\phi_s)^2 = 4(\nabla\phi_s)^2$ we obtain the following equation for the evolution of the phase field:

$$\begin{aligned} \partial_t\phi_s = &\frac{f}{2}\left(\frac{1}{2}(1-2\phi_s)(\nabla\phi_s)^2 + \frac{1}{2}\phi_s(1-\phi_s)\,\nabla^2\phi_s - \phi_s(1-\phi_s)(2\phi_s-1)\right) \\ &-\frac{f}{2}\frac{T'}{T_w}\left(\phi_s(1-\phi_s) - \frac{1}{2}(\nabla\phi_s)^2 + \frac{1}{2}\phi_s(\phi_s-1)\,\nabla^2\phi_s\right) \end{aligned} \tag{22}$$

Comparing this equation with Eq. (8) some differences are obvious. In addition to the second order derivative of the phase-field the square of the

first order derivative appears. Keeping in mind that the $\nabla^2\phi_s$ term stems from the bending term in the free energy expression of the field theoretical approach, the additional derivative implies a different bending term in the free energy of the system: $\mathcal{Q}(\phi_s)(\nabla\phi_s)^2$ instead of just $\xi(\nabla\phi_s)^2$.[17] ξ is a measure for the length scale and $\mathcal{Q}(\phi_s)$ is a function to be determined. The length scale is not explicitely defined in our model. The second difference between Eq. (22) and Eq. (8) is the appearence of phase-field derivatives in the temperature term. This is an effect of our growth model and the discreteness of the lattice but the physical background is not yet clear. In the field-theoretical approach of the phase-field model, the phase-field ϕ is regarded as a mean field and the correlation length becomes very large near the transition point,[23] whereas the correlation length in the solidification/melting transition is small. In our lattice model the phase-field can be locally very sharp and might include higher order terms of interaction. A more detailed analysis of the model is under investigation.

Equations (12) and (14) do not include anisotropy effects. For computing the growth of dendrites we have to account for such effects and therefore we modify the equations. Firstly, we introduce a new (local) lattice with directions $\tilde{i}$, which might be tilted by an angle $0 \leqslant \alpha \leqslant \pi/4$ against the lattice for hydrodynamic calculations. We restrict the variation of α because we will consider later only crystals with a four-fold symmetry. For convenience we introduce a parameter $a_\alpha = \alpha 4/\pi$, which varies between 0 and 1. The new local lattice presents crystal structure so that crystal axes do not need to coincide with the axes of the lattice for the lattice fluid. The introduction of a new lattice would in principle allow us to calculate the growth of different crystals with different orientations of their symmetry axes.

A crystal will grow normal to its local interface. In continuum phase-field models growth direction and interface curvature are computed from the phase field by first and second order derivatives (see, e.g., ref. 3). This type of computation is not appropriate for our mesoscopic phase-field model for two reasons: first, overnext neighbours have to be included in the algorithm, which would slow down the computation especially on parallel platforms. Secondly and more important, the transition region of the phase-field might be very sharp so that derivatives could be computed only after a time-consuming smoothing procedure. Therefore, we do not calculate the direction of the growth direction but only the probability that, for every direction $\tilde{i}$, the growth occurs along $\tilde{i}$. For this purpose we compute at node $\vec{r}_*$ for every direction $\tilde{i}$:

$$\begin{aligned} G_{\tilde{i}} = {} & (\phi(\vec{r}_* + \vec{d}_{\tilde{i}}) - \phi(\vec{r}_* - \vec{d}_{\tilde{i}})) \\ & \times (2 - |\phi(\vec{r}_* + \vec{d}_{\tilde{i}'}) - \phi(\vec{r}_* - \vec{d}_{\tilde{i}'})|) \\ & \times (2 - |\phi(\vec{r}_* + \vec{d}_{\tilde{i}'}) - \phi(\vec{r}_*)|)(2 - |\phi(\vec{r}_* - \vec{d}_{\tilde{i}'}) - \phi(\vec{r}_*)|) \end{aligned} \tag{23}$$

$\tilde{i}'$ denotes the direction perpendicular to direction $\tilde{i}$ and $\vec{d}_{\tilde{i}}$ is a vector of unit length in direction $\tilde{i}$. The values at $\vec{r}_* + \vec{d}_{\tilde{i}}$ are computed by bilinear interpolation. The growth probability in direction $\tilde{i}$ is given by $2G_{\tilde{i}}/\sum_{\tilde{i}} |G_{\tilde{i}}|$, if $G_{\tilde{i}}$ is positive. If $G_{\tilde{i}}$ is negative the crystal will melt. Obviously, if a crystal grows in a certain direction with a certain probability, it will melt in the opposite direction with the same probability. So we count every probability twice in the sum and the factor 2 in the numerator counteracts this. At last we define a growth factor, which includes the local phase-field and the anisotropy $\epsilon_{\tilde{i}}$ $(0 \leqslant \epsilon_{\tilde{i}} \leqslant 2)$:

$$\tilde{\phi}_{\tilde{i}} = \begin{cases} \dfrac{2G_{\tilde{i}}}{\sum_{\tilde{i}} |G_{\tilde{i}}|} \left\{ \dfrac{1}{2} (1 - \phi(\vec{r}_*)) \right\}^2 \epsilon_{\tilde{i}} & \text{if} \quad G_{\tilde{i}} \geqslant 0 \\ \dfrac{2G_{\tilde{i}}}{\sum_{\tilde{i}} |G_{\tilde{i}}|} \left\{ \dfrac{1}{2} (1 + \phi(\vec{r}_*)) \right\}^2 & \text{if} \quad G_{\tilde{i}} < 0 \end{cases} \tag{24}$$

Now we have to transform $\tilde{\phi}_{\tilde{i}}$ back on the lattice directions via $\tilde{\phi}_i = \{(1-a_\alpha)\,\tilde{\phi}_{\tilde{i}} + a_\alpha \tilde{\phi}_{\tilde{i}-1}\}\, g_i$ where we count i in the same direction as the translation of i into $\tilde{i}$. The factor g_i recognizes if i is a diagonal direction $(g_i = 1/\sqrt{2})$ or a horizontal/vertical one $(g_i = 1)$. Equations (12) and (13) are modified into:

$$K^{s \to l}(r_*, t_*) \to K^{s \to l}(r_*, t_*) \tfrac{1}{8} \sum_i \max\{-\tilde{\phi}_i(\vec{r}_* - \vec{c}_i')), 0\} \tag{25}$$

$$K^{l \to s}(r_*, t_*) \to K^{l \to s}(r_*, t_*) \tfrac{1}{8} \sum_i \max\{+\tilde{\phi}_i(\vec{r}_* - \vec{c}_i')), 0\} \tag{26}$$

Due to the definition in Eq. (23) a positive or negative $\tilde{\phi}$ means growth or melting in this direction, respectively. The continuum limit for the anisotropic growth model is quite more complicated, because we have to include the probabilities $G_{\tilde{i}}$ into the expansion. A detailed analysis will be published elsewhere.

Latent heat release results in a change $\delta T_{\mathscr{L}} = -(\Delta T^*/St)(\delta\phi/2)$ of the temperature at node $\vec{r}_*$. Here $St = c_p \Delta T/L$ is the Stefan number, ΔT^* and ΔT are the characteristic temperature differences of the system in lattice and physical units, c_p is the specific heat and L is the latent heat. The minus sign recognizes the fact that heat is released in the solidification process $(\delta\phi < 0)$ and absorbed in the melting process $(\delta\phi > 0)$. The latent heat release acts as an extra force in the direction of u_4 and enters Eq. (3) as an additional force.

The fluid-solid interaction is represented by an empirical mesoscopic force, $\vec{F}^{fs} = -\omega\vec{u}(1-\phi)/2$, whose task is to enforce no flow in the solid phase. To achieve this purpose the relaxation parameter ω has to be chosen

of order 1, i.e., faster than any other process.[24] Note that the force vanishes in the liquid phase ($\phi = 1$). The buoyancy force $\vec{F}^B$, introduced in the last section, has to be slightly modified into $\vec{F}^B = \beta T^* \vec{n}_g (1+\phi)/2$. This excludes the buoyancy force from solid regions.

4. GROWTH OF DENDRITES

We have performed a series of two-dimensional calculations for the growth from a circular seed of radius $r = 3$ l.u. into an undercooled melt. We measure all parameters in lattice units (l.u.): the length scale is the number of nodes, the time scale the number of iterations, and the temperature is defined by its value at the boundaries. The computational domain was 200×200 l.u. and 400×400 l.u. The temperature at the boundary was fixed to $T_b = -0.001$ l.u. The critical temperature was set to $T_c = 0.0$ l.u. and the temperature at the starting time $t = 0$ was $T_{init} = -0.001$ l.u. Firstly, we test if the shape of the dendrite is independent of the tilting angle α. In one case we set $\alpha = 0$, $\epsilon = 0.5$ in diagonal directions and $\epsilon = 1.5$ in horizontal and vertical directions. In the second we set $\alpha = \pi/4$, $\epsilon = 1.5$ in diagonal directions and $\epsilon = 0.5$ in horizontal and vertical directions. This should give exactly the same result and indeed we found identical phase fields. The crystal axes can be also tilted by a more arbitrarly angle like, e.g., $\alpha = 0.625\pi$. As expected we still obtain the same dendrite structure.[24]

Secondly, we compare the shape and growth rate with analytical results according to the solvability theory.[1, 25, 26] This theory assumes a parabolic shape of the dendritic tip and treat the diffusion problem quasistationary. With these assumptions a simple stability criterion for the growth of a tip can be deduced. Furthermore, it is stated that the stability criterion $\sigma^* = 2d_0 D/\rho_{tip}^2 v_{tip} = (\tilde{\rho}_{tip}^2 \tilde{v}_{tip})^{-1}$ depends only on the anisotropy and the tip Péclet number $Pe = \rho_{tip} v_{tip}/2D = \tilde{\rho}_{tip} \tilde{v}_{tip}$ depends only on the undercooling.[1] Here $d_0 = \Gamma St/\Delta T$ is the capillary length, $\tilde{v}_{tip} = v_{tip} d_0/2D$ the dimensionless dendritic growth velocity, and $\tilde{\rho}_{tip} = \rho_{tip}/d_0$ the dimensionless tip radius. In Table I we list the Péclet numbers and values of σ^* for our calculations. The anisotropy was the same in all calculations ($\epsilon = 1.5$ in diagonal and $\epsilon = 0.5$ in horizontal or vertical direction). For the same undercooling the Péclet numbers are of the same order but the agreement is not very satisfactory. One reason for this discrepancies might be an uncertainty in the tip radius, which was computed geometrically. This might be not very accurate. A computation directly from the phase-field values will be developed. σ^* shows even a higher variation from calculation to calculation though according to the solvability theory it should be identical, because the anisotropy is the same in all cases. Besides the already mentioned problem of determining the tip radius, the more severe

Table I. Parameters and Results for Numerical Calculations of Dendritic Growth. Calculation 1 Was Performed on a 200×200 Grid, All Others on a 400×400 Grid. St_I and St_T Are the Undercoolings, Calculated from $\tilde{\rho}_{tip}$ and $\tilde{v}_{tip}$ with the Ivantsov and the Temkin Model, Respectively. All Parameters Are in Lattice Units (l.u.)

No.	D	T_w	T_s	f	St	δ	v_{tip}	ρ_{tip}	d_0	Pe_{tip}	σ^*	St_I	St_T
1	0.25	1×10^{-4}	1×10^{-4}	0.1	0.1	1.0	3.3×10^{-3}	3.3	5.0×10^{-3}	1.5×10^{-3}	0.1	0.07	0.09
2	0.25	2×10^{-4}	1×10^{-4}	0.1	0.1	0.8	9.6×10^{-4}	5.6	1.3×10^{-2}	1.1×10^{-2}	0.2	0.05	0.07
3	0.25	3×10^{-4}	1×10^{-4}	0.1	0.05	0.8	3.2×10^{-4}	5.0	8.7×10^{-3}	3.2×10^{-3}	0.6	0.02	0.04
4	0.025	3×10^{-4}	1×10^{-4}	1.0	0.05	0.8	4.2×10^{-5}	3.6	8.7×10^{-3}	2.5×10^{-3}	0.8	0.02	0.05

uncertainty is due to the Gibbs–Thomson coefficient, which is computed using Eq. (20). A quantitative assessment of the approximation inherent to Eq. (20) needs to be developed.

For a particular undercooling $\tilde{\rho}_{tip}$ and $\tilde{v}_{tip}$ have defined relation according to the theory. For small values of $\tilde{\rho}_{tip}$ the relation depends on the theoretical approach. The important ones are the Ivantsov and the Temkin approach.[1] Instead of calculating the (theoretical) dimensionless tip velocity from the measured dimensionless radius and undercooling we find it more convenient to recompute the (theoretical) undercooling from the measured dimensionless tip radius and velocity. Due to the high anisotropy $\tilde{\rho}_{tip}$ is rather small, i.e., we are in a regime where the theoretical approaches differ from each other. The theoretical undercooling computed with the Temkin model is only in reasonable agreement with the value used in our calculations. Again uncertainties in ρ_{tip} and Γ may be a reason.

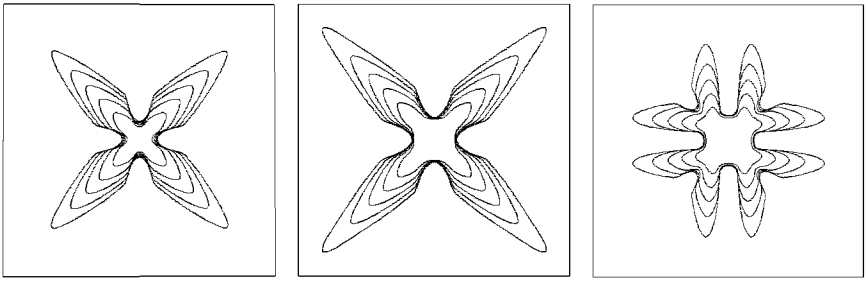

Fig. 2. Evolution of crystal shape ($\phi = 0$) for different seeds and tilting angles α in the case of diffusive transport only. The used parameters are listed in Table I under run No. 3. Isolines ($\phi = 0$) are shown for iterations 30000, 60000, 90000, 120000, and 150000. (a) Spherical seed ($\varnothing = 6$), $\alpha = \pi/4$. (b) Square seed ($l = 40$), $\alpha = \pi/4$. (c) Square seed ($l = 40$), $\alpha = 0$.

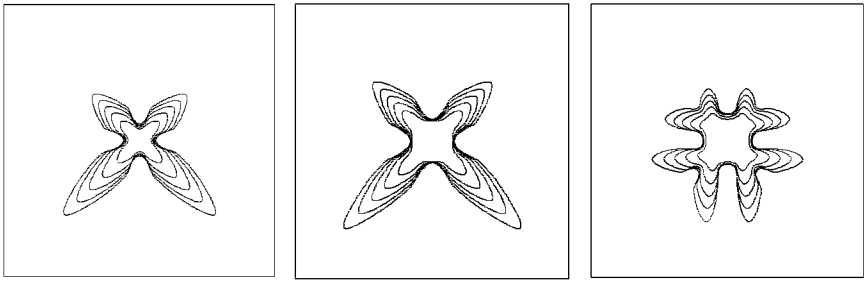

(a) (b) (c)

Fig. 3. Evolution of crystal shape for different seeds and tilting angles α if buoyancy convection is present ($Gr = 4.1 \times 10^6$, $Pr = 2$). The other parameters are listed in Table I under run No. 3. Isolines ($\phi = 0$) are shown for iterations 20000, 40000, 60000, 80000, and 100000. (a) Spherical seed ($\varnothing = 6$), $\alpha = \pi/4$. (b) Square seed ($l = 40$), $\alpha = \pi/4$. (c) Square seed ($l = 40$), $\alpha = 0$.

The structure of the growing dendrite depends on the shape of the seed (see Fig. 2). We start from a circular seed of a diameter $\varnothing = 6$ l.u. and a square of side length $l = 40$ l.u., both positioned at the center. For the latter we performed two calculations, one with no tilt ($\alpha = 0$) and one with a tilt of $\alpha = \pi/4$. The tilted case exhibits the same four-branch structure as the case starting from a circular seed whereas in the untilted case eight branches are formed—each corner acts like an own seed (see Figs. 2b and 2c). Because there are two branches close to each other, the tip growth velocity is a little bit smaller than in the other two cases

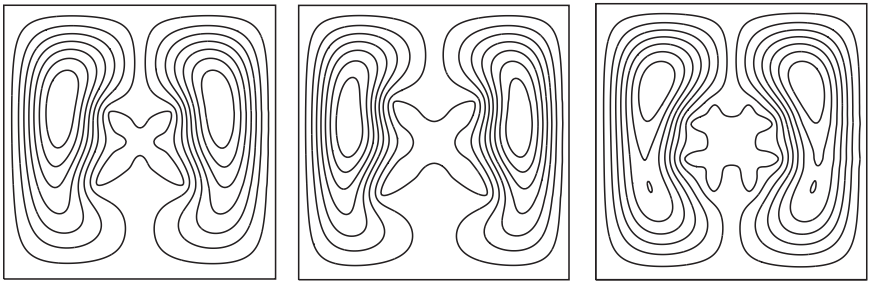

(a) (b) (c)

Fig. 4. Crystal shape and streamlines at iteration 50000 for different seeds and tilting angles α if buoyancy convection is present ($Gr = 4.1 \times 10^6$, $Pr = 2$). The other parameters are listed in Table I under run No. 3. The flow is upstream near the crystal and downstream at the left and right boundary. (a) Spherical seed ($\varnothing = 6$), $\alpha = \pi/4$. (b) Square seed ($l = 40$), $\alpha = \pi/4$. (c) Square seed ($l = 40$), $\alpha = 0$.

($v_{tip} = 7.4 \times 10^{-4}$ l.u.), but the tip radius is slightly larger ($\rho_{tip} = 6.1$ l.u.), resulting in nearly the same Péclet number.

We also investigate the influence of buoyancy convection on the dendrite structure. The buoyancy flow is induced by the heated crystal in the box, the characteristic numbers are the Grashof number $Gr = 4.1 \times 10^6$ and the Prandtl number $Pr = 2$. At the boundaries of the box we set non-slip conditions. From Figs. 3 and 4 it can be seen that the dendrite branches grow faster in the direction of gravity as it was observed by Bänsch and Schmidt.[5]

5. CONCLUSIONS

The growth of dendrites can be calculated within the framework of the lattice Boltzmann method. Hydrodynamics and heat transport is handled by the well-established lattice Boltzmann method with a linear collision matrix on a face-centred hypercubic lattice. The phase transition is described by a rate equation. In order to include the crystal anisotropy a growth parameter was defined. For the isotropic model it was shown that the continuum limit becomes in the leading order the ordinary phase-field equation but without the term of the phase-field bending. By this continuum limit the parameters of the lattice Boltzmann model, like T_w, T_s, and f can be related to the parameters of the ordinary phase-field model, like the Gibbs–Thomson and kinetic coefficient and the width of the transition region. Using these relationsships the dimensionless tip velocity and radius can be computed from the measured ones. This enables us to compare the numerical observed data with the predicted values by the solvability theory. The agreement is quite reasonable. Nevertheless, there are several open questions. The continuum limit for the anisotropic model has not yet been derived and it is not yet clear if the assumption on the temperature relations ($T' \ll T_s, T' \ll T_w$) is applicable.

We have presented the influence of the seed on the growing dendrite and the influence of a moderate buoyancy convection. A more systematic study of parameter variation is required. Especially, the question arises if side-branches will be formed. Calculations on larger lattices with stronger buoyancy convection will be performed. Since they demand significantly more computer power and since it is that LBM codes are very efficient on parallel platforms[27, 28] we are going to set up a parallel version of the current LBM.

ACKNOWLEDGMENTS

Financial support from ESF-PESC Scientific Programme "Challenges in molecular simulations: Bridging the length and time scale gap" is kindly

acknowledged. We wish to thank Prof. M. Mareschal for enlightening discussion and kind hospitality at CECAM.

REFERENCES

1. J. S. Langer, *Rev. Mod. Phys.* **52**:1 (1980).
2. M. E. Glicksman and S. C. Huang, *Convective Heat Transport and Instability Phenomena*, J. Zierep and Ortel, eds. (Braun, Karlsruhe, 1982).
3. C. Beckermann, H.-J. Diepers, I. Steinbach, A. Karma, and X. Tong, *J. Comput. Phys.* **154**:468 (1999).
4. R. Tönhardt and G. Amberg, *J. Crystal Growth* **194**:406 (1998).
5. E. Bänsch and A. Schmidt, *Interfaces and Free Boundaries* **2**:95 (2000).
6. D. M. Anderson, G. B. McFadden, and A. A. Wheeler, *Physica D* **151**:305 (2001).
7. U. Frisch, D. d'Humière, B. Hasslacher, P. Lallemand, Y. Pomeau, and J.-P. Rivet, *Complex Systems* **1**:649 (1987).
8. F. Higuera, S. Succi, and R. Benzi, *Europhys. Lett.* **9**:345 (1989).
9. H. Chen, S. Chen, and W. H. Matthaeus, *Phys. Rev. A* **45**:R5339 (1992).
10. W. Miller, *Phys. Rev. E* **51**:3659 (1995).
11. R. Benzi, S. Succi, and M. Vergassola, *Phys. Reports* **222**:145 (1992).
12. A. Calì, S. Succi, A. Cancelliere, R. Benzi, and M. Gramignani, *Phys. Rev. A* **45**:5771 (1992).
13. F. Massaioli, S. Succi, and R. Benzi, *Europhys. Lett.* **21**:305 (1993).
14. F. Massaioli, R. Benzi, S. Succi, and R. Tripiccione, *Europ. J. Fluid Mech.* **14**:1 (1995).
15. Y. Chen, H. Ohashi, and M. Akiyama, *J. Stat. Phys.* **81**:71 (1995).
16. G. Vahala, P. Pavlo, L. Vahala, and N. S. Martys, *Int. J. Mod. Phys. C* **9**(8):1247 (1998).
17. G. Caginalp, *Applications of field theory to statistical mechanics*, L. Garrido, ed., Lecture Notes in Physics, Vol. 216 (Springer-Verlag, Berlin, 1985), pp. 216–226.
18. G. Caginalp, *Ann. of Phys.* **172**:136 (1986).
19. G. McFadden, A. A. Wheeler, R. J. Braun, S. R. Coriell, and R. F. Sekerka, *Phys. Rev. E* **48**(3):2016 (1993).
20. A. Karma and W.-J. Rappel, *Phys. Rev. E* **57**(4):4323 (1998).
21. J. J. Egglestone, G. B. McFadden, and P. W. Voorhees, *Physica D* **150**:91 (2001).
22. A. A. Wheeler, W. J. Boettinger, and G. B. McFadden, *Phys. Rev. A* **45**(10):7424 (1992).
23. G. Caginalp and E. Socolowsky, *SIAM J. Sci. Comput.* **15**(1):106 (1994).
24. W. Miller, S. Succi, and D. Mansutti, *Phys. Rev. Lett.* **86**(16):3578 (2001).
25. J. S. Langer, *Phys. Rev. A* **33**:435 (1986).
26. P. Pelcé, *Dynamics of Curved Fronts* (Academic Press, New York, 1988).
27. G. Punzo, F. Massaioli, and S. Succi, *Comput. Phys.* **5**:1 (1994).
28. W. Miller and S. Succi, *Computational Fluid Dynamics '96*, J.-A. Désidéri, C. Hirsch, P. Tallec, M. Pandolfi, and J. Périaux, eds., ECCOMAS (John Wiley & Sons, 1996), pp. 1052–1058.